55. T. Guillot and B. Gladman, unpublished data.
56. W. B. Hubbard, *Icarus* **137**, 196 (1999). See also the proposed NASA discovery mission INSIDE (http://INSIDEJupiter.lpl.arizona.edu/).
57. Two space missions are dedicated to the photometric detection of transits: COROT, a mission of the *Centre National d'Etudes Spatiales*, due to be launched in 2003 (http://www.astrsp-mrs.fr/www/pagecorot/html); and KEPLER, a NASA project (http://www.kepler.arc.nasa.gov/).
58. E. Anders and N. Grevesse, *Geochim. Cosmochim. Acta* **53**, 197 (1989).

59. I thank D. Saumon, B. Gladman, and S. Cazaux for many comments on the manuscript and S. Atreya, D. Gautier, B. Hubbard, A. Morbidelli, T. Owen, and D. Stevenson for stimulating discussions. This research was supported by CNRS (*Action Thématique Innovante* and *Programme National de Planétologie*).

REVIEW

The Galilean Satellites

Adam P. Showman[1] and Renu Malhotra[2]

NASA's Galileo mission to Jupiter and improved Earth-based observing capabilities have allowed major advances in our understanding of Jupiter's moons Io, Europa, Ganymede, and Callisto over the past few years. Particularly exciting findings include the evidence for internal liquid water oceans in Callisto and Europa, detection of a strong intrinsic magnetic field within Ganymede, discovery of high-temperature silicate volcanism on Io, discovery of tenuous oxygen atmospheres at Europa and Ganymede and a tenuous carbon dioxide atmosphere at Callisto, and detection of condensed oxygen on Ganymede. Modeling of landforms seen at resolutions up to 100 times as high as those of Voyager supports the suggestion that tidal heating has played an important role for Io and Europa.

Jupiter's four large moons, Io, Europa, Ganymede, and Callisto, are collectively known as the Galilean satellites after Galileo Galilei, who discovered them in 1610. Their discovery overturned the Western worldview of an Earth-centered universe. The first quantitative physical studies of these worlds became possible during the 19th century when Simon de Laplace derived the satellite masses from their mutual gravitational perturbations and, subsequently, other workers used a new generation of telescopes (at Yerkes and Lick observatories in the United States) to measure the sizes of these moons. These data yielded estimates of bulk density good to a few tens of percent and revealed the trend of decreasing density from the inner to the outer satellites (Table 1). More recent observations of water ice on the surfaces of the outer three moons led to the inference that the satellite compositions range from mostly silicate rock at Io to 60% silicate rock and 40% volatile ices (by mass) at Ganymede and Callisto (*1*). This trend probably reflects conditions within the protojovian nebula at the time the satellites formed (*2*). The Voyager flybys of Jupiter in 1979 revealed evidence of substantial geological activity on these distant worlds (*3*–*6*). The observed activity on Io is powered by the tidal distortions of Io's figure caused by the strong gravity of Jupiter, and Europa's fractured terrains also probably result from tidal heating and flexing. Because the rotation rates are synchronized with the orbital motions, the tides oscillate in amplitude and orientation only because of the satellites' eccentric orbits. The orbital eccentricities of Io, Europa, and Ganymede are excited to nonzero values by resonant gravitational forces between the three satellites (*7*). In turn, the stability of the resonant orbital configuration (called the Laplace resonance) is controlled by the rate of dissipation of tidal energy within the satellites. Thus, the geologic evolution of these satellites is intimately coupled to their orbital configuration. Embedded within Jupiter's radiation belts, all four satellites are also bombarded by energetic particles that cause chemical reactions and physical erosion that are alien from a terrestrial perspective. These satellites rival the terrestrial planets in complexity but embody processes foreign to our Earth-based experience.

The Galileo spacecraft is performing a 4-year orbital tour scheduled to end in late 1999. By the end of the tour, the spacecraft will have completed over 20 orbits of Jupiter, most arranged to make a close flyby past one of the four Galilean moons. Flyby distances of as little as 200 km have allowed new images with resolution of up to 10 m/pixel to be acquired. (In contrast, Voyager's best resolution was 500 m/pixel.) Qualitatively new constraints have been obtained by a suite of additional experiments: Doppler tracking of the spacecraft's radio signal allowed gravitational moments (hence moments of inertia) to be calculated, a magnetometer provided measurements of the moons' magnetic fields, plasma and energetic particle detectors constrained the electrical and magnetic properties of the moons and their environs, and three spectrometers obtained spatially resolved spectra of the moons' surfaces from the ultraviolet to the far infrared (IR) (*8*). Although the data stream was limited by failure of the high-gain antenna (which, for example, allowed just a few percent of each satellite's surface to be imaged at resolutions exceeding 200 m/pixel), the nature of the data sets is so unique that the measurements have boosted our understanding and raised numerous new questions. Concurrently, observations from ground-based facilities and the Earth-orbiting Hubble Space Telescope (HST) have yielded important discoveries.

Callisto

Unlike Io, Europa, and Ganymede, Voyager showed Callisto to be a heavily cratered body apparently devoid of endogenic volcanic or tectonic landforms (*6*). Primary interest in Callisto has centered on comparison with Ganymede, which has similar bulk properties but a highly tectonized surface. Callisto's mean density suggests roughly equal masses of rock and ice, but early opinions differed about whether the interior contained a primordial, undifferentiated mixture of the two components or a differentiated ice mantle overlying a silicate rock and iron core (*1*, *5*). Callistan craters are flatter (and often display a distinctive morphology) compared with their terrestrial counterparts, indicating that the uppermost 10 km is mechanically dominated by ice rather than rock (*9*, *10*), supporting the idea of at least partial differentiation of Callisto's interior. IR spectra of the surface contain numerous water ice absorption features, but the low albedo and existence of other nonice features (*11*) imply contamination by darker material. Radiative transfer retrievals of the spectra have yielded mean ice mass fractions of the uppermost ~1 mm ranging from 10 to ~50%, with some regions recognized as essentially ice free (*5*, *12*, *13*).

Interior structure and magnetic field. From Galileo tracking data, Callisto's moment of inertia has been determined to be $C/MR^2 = 0.359 \pm 0.005$, which is 4 standard deviations less than 0.38, the value expected for a homogeneous rock and ice body of Callisto's mass and radius (*14*). Three-layer interior models suggest the existence of a central silicate core up to 50% of Callisto's

[1]Department of Mechanical Engineering, University of Louisville, 215 Sackett Hall, Louisville, KY 40292, USA. E-mail: showman@flolab.spd.louisville.edu [2]Lunar and Planetary Institute, 3600 Bay Area Blvd., Houston, TX 77058, USA. E-mail: renu@lpi.jsc.nasa.gov

radius in size, an intermediate rock and ice layer with a density of 1.7 to 2.4 g cm^{-3}, and an outermost ice layer 0 to 500 km thick with a density of 0.9 to 1.3 g cm^{-3} (*15*). Within these ranges, larger cores correspond to lower middle layer densities and thinner upper layers. It is difficult to rule out either completely differentiated or undifferentiated models, however. For example, nonhydrostatic mass anomalies could cause a differentiated Callisto to appear partially differentiated or even undifferentiated (*16*).

Magnetic field data from three Galileo flybys show that Callisto has a distinct magnetic field signature (*17*). Long-wavelength structure from data for two of the flybys, C3 and C9, is fit well by the expected response of a perfect conductor in Jupiter's time-variable field. In contrast, a dipole with fixed orientation (relative to Callisto's figure) does not match data for these two flybys. The good fit of the induced dipole model suggests that Callisto contains an internal conducting layer. The conductivity of solid ice is too low, and a hypothetical metallic core is too far below the surface, but an internal ocean 10 km thick would have the required conductance if the water has the salinity of terrestrial seawater (*17*, *18*). However, data from the third flyby (C10) are dominated by short-wavelength fluctuations, plausibly resulting from plasma effects (*17*), and appear to be inconsistent with any dipole model.

Maintaining an ocean in Callisto today requires either stiffer ice rheology than has generally been assumed (to lower the convective heat flux at a given interior temperature and prevent the interior from cooling below the 251 K minimum in the water-ice melting curve over solar system history) or the existence of an antifreeze in the ocean. For the latter, ammonia is perhaps the best such candidate, depressing the freezing temperature by nearly 100 K (*19*); salts probably cause an insufficient depression of the melting temperature (*20*). Models including trace quantities of ammonia have long suggested the possibility of present-day oceans in Ganymede and Callisto (*21*). However, reconciling partial differentiation with the existence of an ocean is difficult: Some portion of the uppermost ice layer must remain at the melting temperature to the present day, and the mixed ice-rock layer must never have attained the melting temperature. Moreover, partial differentiation is puzzling because once differentiation starts, the melting tends to drive the process to completion (*22*).

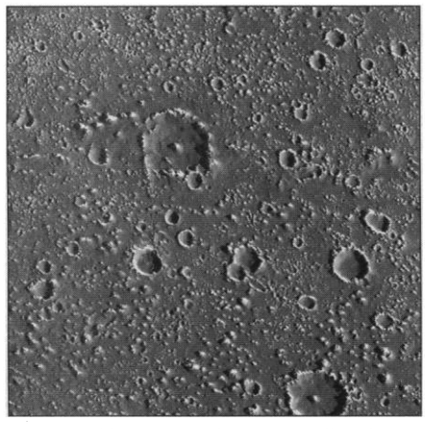

Fig. 1. Galileo image depicting Callisto's cratered terrain. The image spans an area 75 km across with a resolution of 87 m/pixel. Smooth, dark material blankets regions between and within many of the craters, and the terrain has fewer small craters (relative to its number density of large craters) than occur on Ganymede or the moon.

Surface and atmosphere. Galileo near infrared mapping spectrometer (NIMS) data have revealed several new spectral absorption bands and confirmed the suggestion that the surface contains an average of 50% ice or less, including some ice-free regions (*23*, *24*), but the composition of the nonice constituents remains uncertain. A spatially widespread 4.25-μm wavelength feature has been tentatively identified as CO_2 ice. But a problem with this hypothesis is that CO_2 ice would sublimate rapidly at Callisto's low-latitude 165 K noontime temperatures. To resolve this issue, McCord *et al.* (*23*) suggested that the CO_2 occurs in interstitial spaces or fluid inclusions containing only a few molecules each; they pointed out that laboratory spectra of several minerals show similar absorption bands from this effect. Additional weaker surface features at 4.57, 4.05, 3.88, and 3.4 μm also exist in NIMS data and have been suggested to be C≡N (or perhaps CO), SO_2, H_2CO_3 (or perhaps S−H), and the C−H bond (*23–25*). HST and International Ultraviolet Explorer measurements also indicate sulfur, possibly in the form of SO_2 (*26*). Furthermore, NIMS observations taken above Callisto's limb show a weak 4.25-μm absorption within 100 km of Callisto's surface, which constitutes tentative evidence for a CO_2 atmosphere with surface pressure of 10^{-6} Pa (*27*). This interpretation implies atmospheric CO_2 in equilibrium with CO_2 ice at 75 K, such as a CO_2 ice reservoir near the poles where temperatures remain low. Hypothetical sources for the CO_2 are conversion of organics [perhaps supplied from meteoroids (*23–25*, *28*)] or degassing from the interior (*27*).

Geology. Analyses of Galileo images indicates that in some regions Callisto has been subject to intense surface degradation at scales smaller than 1 km (*29*). At these scales, many of Callisto's surface features appear substantially more degraded than those on Ganymede's dark terrain. In many cases, the nature of the degradation appears qualitatively different than on Ganymede or the moon (*29*, *30*). Rather than appearing "softened," old kilometer-scale impact craters on Callisto often appear to be broken up by disaggregation into large blocks. Intercrater plains typically appear quite dark and smooth (Fig. 1). Furthermore, the number density of small (<3 km diameter) craters on Callisto is less than on Ganymede, the reverse of the situation for larger (>10-km diameter) craters (*31*). Because the size distribution of impactors is not expected to be different for the two moons, it appears that small craters on Callisto are preferentially lost by some erosional process. Moore *et al.* (*29*) suggest that erosion driven by sublimation has modified the landscape; they invoke the presence of an ice more volatile than H_2O, which they suggest to be CO_2 on the basis of the putative detection of atmospheric and surface CO_2. Although degassing might provide enough CO_2, conversion of organics probably could not. Ammonia ice is an attractive alternative because its absence at Ganymede would be the natural result of higher temperatures in the protojovian nebula there relative to Callisto (*21*). Semiquantitative modeling demonstrates the plausibility of scarp retreat, pit formation, and other sublimation-related effects (*29*, *32*), although the detailed morphologies of craters and other degraded features have not been quantitatively explained.

Ganymede

Ganymede, which exceeds Mercury and Pluto in diameter and is the solar system's largest satellite, was revealed by Voyager to have a

Table 1. Galilean satellite physical parameters.

Parameter	Io	Europa	Ganymede	Callisto
Mass, M (10^{23} kg)*	0.8932	0.480	1.482	1.076
Mean radius, R (km)†	1818.1 ± 0.1	1560.7 ± 0.7	2634.1 ± 0.3	2408.4 ± 0.3
Density (g cm^{-3})	3.518–3.549	3.014	1.936	1.839
$C/M R^2$‡	0.371–0.380	0.346 ± 0.005	0.3105 ± 0.0028	0.359 ± 0.005
Intrinsic magnetic field (nT) at equatorial surface§	1300	–	750	–
Ambient jovian magnetic field (nT)‖	1835	420	120	35

*(*110, 70, 34, 14*). †(*120*). Alternate methods give Io radii of 1821.6 ± 0.5 km (*111*) and 1822.7 ± 0.5 km (*120*); the discrepancies are unresolved. ‡(*111, 110, 70, 34, 14*). §(*112, 50*). Io field is tentative. ‖(*121*).

complex geologic history. About 40% of Ganymede's surface is covered by dark, heavily cratered terrain, and the remainder consists of heavily tectonized bright terrain with relatively low crater densities, indicating the occurrence of a major geologic upheaval long after the formation of the cratered plains (*6*). The question of what caused these "grooved" terrains (Fig. 2) and why Callisto escaped such a turbulent history has become a major puzzle in planetary science (*5*). Ganymede's mean density (Table 1) suggests comparable masses of rock and ice; formation and evolution models have long suggested differentiation into an ice mantle overlying a silicate rock and iron core (*1*). Analysis of Ganymede's IR spectra and visible albedo indicated a surface mainly covered by water ice, with 50 to ~90% ice by mass (*5*, *12*, *13*). Crater morphologies indicated that the mechanical properties of the surface are dominated by the rheology of ice (*9*). Ganymede's grooved terrains were generally thought to have formed by volcanic emplacement of liquid water or soft ice within a global set of graben (*5*), although the emplacement and groove formation processes were poorly understood. Crater dating suggests that these events occurred as recently as 1 billion years ago, although factor of three uncertainties exist (*33*).

Interior structure. Analysis of Galileo data from two close flybys shows that Ganymede's axial moment of inertia is $C/MR^2 = 0.3105 \pm 0.0028$, the smallest measured value for any solid body in the solar system (*34*). This value indicates that the density increases with increasing depth inside Ganymede. Three-layer models, constrained by plausible hypotheses for their compositions, indicate that Ganymede is differentiated into an outermost ~800-km-thick ice layer of ~1 g cm^{-3} density and an underlying silicate mantle of ~3 to 4 g cm^{-3} density. A central core of Fe or FeS (with density in the range of 5 to 8 g cm^{-3}) with a radius as large as 50% of Ganymede's radius is allowed, but not required, by the data. The existence of Ganymede's magnetic field, however, suggests the presence of such a metallic core.

Geology. Galileo images indicate that Ganymede underwent a more violent tectonic history, with a less obvious role for cryovolcanism, than had been assumed during the Voyager era (Fig. 2). (Cryovolcanism refers to volcanism that occurs in icy materials rather than rock.) Much of Ganymede's bright terrain is heavily tectonized at all scales exceeding tens of meters (*35*–*37*). Some narrow lanes seen in Galileo images appear to have undergone extensional strains exceeding 50% (*37*, *38*). The violence of this newly observed high-strain tectonism is exemplified by regions where grooved terrains cross cut craters, which show that the crater rims become nearly unrecognizable when the extensional strains exceed 30 to 50% (*38*). In contrast, during the Voyager era, grooves had been generally assumed to result from horst-and-graben faulting, with implied strains of just 0 to 2% (*39*). Formation of newer grooved terrain also apparently caused tectonic destruction of underlying, older grooved terrain in some cases (*36*, *40*). Although several small cryovolcanic flow features have been discovered (*41*), there is little evidence for ubiquitous eruptive vents, flow fronts, or other obvious volcanic landforms. These observations suggest that intense tectonic deformation of preexisting terrain could constitute a major resurfacing agent on Ganymede, with cryovolcanism playing a relatively minor role, at least for some portions of bright terrain (*40*). This hypothesis is attractive because it circumvents the difficulty of bringing to the surface large quantities of liquid water or soft ice. Several challenges remain, however. For example, regions where strain exceeds 50% probably constitute only a small fraction of Ganymede's grooved terrain, because no evidence for compressional deformation has been found and the maximum possible (linear) global expansion undergone by Ganymede is probably 1 to 2% (*39*, *42*). Such small strains appear incapable of erasing craters and other preexisting topography. Additional challenges include explaining how the terrain is brightened (*43*) and why ~10^2- to 10^3-km-wide regions of tectonized terrain are typically separated from untectonized regions by zones just 1 to 10 km wide.

Recent modeling and data analysis have shed light on possible formation mechanisms for the grooves. Some regions imaged by Galileo at high resolution appear to have formed by horst-and-graben faulting, as had generally been assumed after Voyager. Other regions, however, contain numerous ~1-km ridges and troughs of triangular cross section that are reminiscent of domino-style tilt-block normal faulting (*36*, *37*); generally, these regions also contain a longer wavelength (~5 to 10 km) undulation (*36*, *37*, *44*). Several authors have hypothesized that the long-wavelength undulations formed by a necking instability in the brittle lithosphere (*45*). Examination of groove stratigraphy suggests that grooves of a given stratigraphic age have consistent directions over hundreds of kilometers, favoring large-scale rather than local stress patterns for groove formation (*46*).

Ganymede's history may have been shaped by tidal heating and flexing from an ancient orbital resonance; this might help explain why Ganymede's surface differs so drastically from Callisto's despite the fact that their evolution is otherwise predicted to be similar (*42*, *47*, *48*). Callisto is not involved in a resonance, neither currently nor in the past, but several plausible ancient orbital configurations could have excited Ganymede's eccentricity to ~0.01 to 0.02 during the past few billion years, producing mean heating up to $10^{17}\ Q_J^{-1}$ W and tidal flexing stresses up to a bar (*42*, *47*). (Q_J is the tidal dissipation factor of Jupiter.) This heating rate is rather modest and exceeds the expected radiogenic heat production only if Q_J is less than 10^5 [which is near its time-averaged lower bound (*49*)]. Dynamical effects can potentially cause the heat to be released in intense, short-period pulses, perhaps generating a massive subsurface ocean, global expansion of ~1%, and consequent lithospheric deformation, but recent modeling tentatively precludes such events (*42*). This does not support the possibility that tidal heating induced bright terrain formation. However, a better comprehension of the requirements for grooved terrain formation is needed before we understand the role of tidal heating for Ganymede.

High-resolution images of the dark terrain suggest that the dark material is a thin lag overlying a lighter substrate and indicate the importance of sublimation in creating this lag and producing albedo heterogeneity (*30*).

Magnetic field. Magnetometer data acquired during four close passes of Galileo past Ganymede have shown that Ganymede has an intrinsic magnetic field strong enough to generate a minimagnetosphere embedded within the jovian magnetosphere (*50*). A model with a fixed Ganymede-centered di-

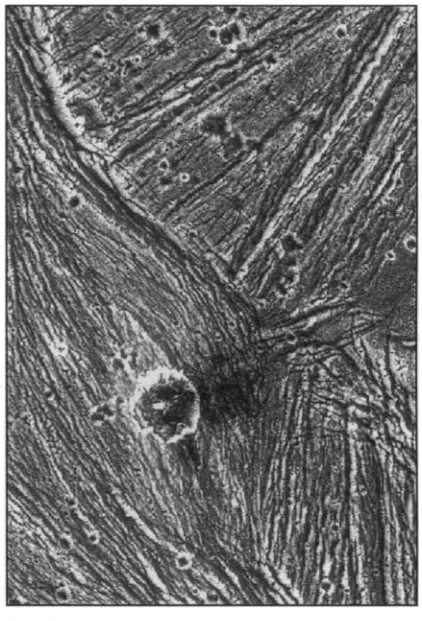

Fig. 2. Galileo image of grooved terrain on Ganymede. The image spans about 59 km by 40 km and illustrates the pervasive tectonism of grooved terrain. The image, with a resolution of ~74 m/pixel, was taken in high sun (low solar incidence angle); the contrast primarily represents albedo differences (*36*, *43*). The circular features are impact craters.

pole superposed on the jovian ambient field provides a good first-order match to the data and suggests equatorial and polar field strengths at Ganymede's surface of 750 and 1200 nT, respectively; these values are 6 to 10 times the 120-nT ambient jovian field strength at Ganymede's orbit. According to this model, magnetic field lines emanating from Ganymede's poles connect to Jupiter, whereas those nearer Ganymede's equator intersect Ganymede's surface at both ends. Detection of numerous electromagnetic and electrostatic waves and measurements of energetic particles close to Ganymede confirm the inference of a magnetosphere (*51*, *52*), although its exact size is debated (*53*). Like most planets with magnetospheres, Ganymede appears to radiate radio waves (*54*).

The mechanisms that generate Ganymede's magnetic field remain enigmatic. Dynamo action in a hypothetical salty ocean is unlikely because unrealistically large convective velocities of $\sim$1 m s^{-1} are required to trigger a dynamo; dynamo action in a liquid Fe-FeS core is more plausible because the required velocities are only $\sim 10^{-5}$ m s^{-1} (*55*). The difficulty lies in understanding how convection occurs at present: The cooling rate required for onset of convection in the core is 400 K per billion years if no inner core of solid Fe exists and is several times less with the presence of an inner core. These values exceed that expected from the gradual decline of the radioisotope heat budget in the overlying silicate, suggesting that the liquid core should cool by conduction alone (*56*). Tidal heating during an ancient orbital resonance does not provide a solution because the resonance is unlikely to substantially affect the core heat budget (*57*). Motivated by these concerns, some workers have suggested remanent magnetization as an alternative source of Ganymede's magnetic field (*58*). The magnetized rocks would be those layers of the silicate mantle that were above the Curie temperature in the past but have since cooled below it. Even this scenario can succeed only if Ganymede had an intrinsic, dynamo-generated field with a surface strength of perhaps 3×10^4 nT in the past. The ancient cooling rate may have been large enough to allow core convection earlier in Ganymede's history, although no studies have been performed to determine whether a dynamo can generate a magnetic field of the required strength.

Surface and atmosphere. Molecular oxygen (*59*) and ozone (*60*, *61*) have been discovered at densities high enough to indicate that they exist within Ganymede's predominantly water-ice surface. The oxygen density peaks at low and midlatitudes, contrary to the expectation for free oxygen ice; solid oxygen is unstable at Ganymede's surface temperatures and, if present, would rapidly migrate to the poles. Perhaps the oxygen is preserved in interstitial spaces containing just a few molecules each (*59*, *62*). An alternative model is that the oxygen exists within tiny, high-density gas bubbles trapped in the ice and that the ozone results from radiolysis of the oxygen (*61*, *63*). Oxygen airglow measurements also indicate the existence of a molecular oxygen atmosphere with column density of 10^{14} to 10^{15} cm^{-2}; such an atmosphere would result naturally from diffusion of the oxygen from the crust (*64*). The oxygen is generally agreed to result from ion and electron bombardment of the water ice, although the channeling influence of Ganymede's magnetic field on the ion fluxes has not been fully considered. Galileo measurements indicate that hydrogen ions and atoms are escaping from Ganymede; if the hydrogen results from the breakup of surface H_2O molecules, the measured escape flux implies formation of an amount of oxygen equivalent to a few meters thickness of solid per billion years (*65*). SO_2 has also been observed on Ganymede's surface (*66*). As with Callisto, NIMS has observed nonice absorptions at 3.4, 3.88, 4.05, 4.25, and 4.57 μm on Ganymede's surface, although these absorptions are weaker than on Callisto (*23*, *24*).

Europa

Voyager showed Europa's surface to be cross cut by numerous lineaments and nearly devoid of large impact craters, suggesting an active geologic history (*4*, *6*). Europa's mean density of 3.0 g cm^{-3} indicates that the interior is predominantly silicate rock, but IR spectral and albedo measurements show that the surface is dominated by water ice, with trace contamination by sulfur and perhaps silicate material (*4*, *67*). Early models suggested that the H_2O layer could range from several to $\sim$100 km in thickness, with the larger values considered more likely. Models of heat loss by solid state convection in the ice suggest that Europa (and other icy satellites) should be able to freeze completely if the main heat source is radiogenic and if the ice lacks trace constituents capable of lowering the freezing point (*68*). However, Europa is tidally heated because of its participation in the Laplace resonance, and this heating may be sufficient to prevent freezing of a primordial ocean. Uncertainties in the ice rheology and tidal heating rate renders this conjecture inconclusive, however (*69*). Crater dating indicates that the surface is $\sim$10 million years old (*33*).

Interior structure. Doppler tracking data acquired during four close flybys of Galileo past Europa revealed that Europa's axial moment of inertia is $C/MR^2 = 0.346 \pm 0.005$, implying a partial condensation of material toward Europa's center (*70*). Three-layer models constrained by plausible compositions suggest that Europa contains an outermost H_2O layer of $\sim$1 g cm^{-3} density and $\sim$80- to 200-km thickness, an intermediate silicate rock mantle, and perhaps an Fe-FeS metallic core. Models without a metallic core are consistent with the data but require high silicate densities of 3.8 g cm^{-3}; more plausible models have a metallic core 30 to 50% of Europa's radius in size and a silicate mantle density of 3.0 to 3.5 g cm^{-3}. Models in which the H_2O layer is much thinner than 80 km require both a silicate mantle density $<$3.0 g cm^{-3} and the existence of a dense metallic core. This latter structure is implausible because such low silicate densities require the silicates to be hydrated; hydrated silicates are only stable below $\sim$1100 K, whereas core formation requires temperatures exceeding $\sim$1350 K. Because the densities of liquid water and ice are similar, the Galileo gravity data cannot be used to infer the phase (solid or liquid) of the H_2O layer.

Geology. Low-resolution ($\sim$2 to 4 km/pixel) images taken by Voyager and Galileo show Europa's surface to be dominated by two terrain types, smooth plains and mottled terrain (Fig. 3), and indicate the existence of a network of long, narrow light and dark bands that give the moon the appearance of a ball of string (*4*, *35*). High-resolution (10 to 200 m/pixel) Galileo images show a diversity of landforms (*71*). The plains generally contain generation after generation of overprinted ridges, and much of the mottled terrain contains chaotic regions of disrupted crustal blocks (dubbed "chaos" terrains) (Fig. 4, A and B). The processes responsible for forming chaos and ridges appear capable of destroying preexisting terrain and therefore resurfacing the satellite (*72*–*74*). Ridges range in complexity from simple ridge pairs to intricate, interbraided complexes surrounded on both sides by diffuse dark tracks $\sim$10 km wide (called triple bands because of their low-resolution appearance as two dark bands separated by a bright medial stripe) (*71*, *75*). Hypotheses for ridge formation include compressional deformation of the lithospheric ice along a fracture (*76*) or pileup of material expelled from the fracture; the stress necessary for the latter process could result from either the compressional phase of the diurnal tide (*75*) or exsolution of gases contained within liquid water in the fracture (*71*, *77*). Linear diapirism is another possible ridge formation mechanism (*78*). The dark portions of triple bands could form by venting of dark debris, ponding of dirty liquid water that subsequently freezes, or metamorphism triggered by an underlying dike of warm ice (*71*, *75*, *79*).

Chaos regions may form by subsurface convective activity, viscous volcanic flows, or locally complete melting of the ice layer (*71*, *73*, *74*, *80*). The latter model makes

several specific predictions that appear qualitatively confirmed by the data (*74*). Several studies suggest that chaos is generally younger than the ridged plains (*73*, *81*), although debate exists (*74*). High- resolution images also reveal the existence of numerous other small (<20 km) landforms, including pits, domes, platforms, irregular lobate features, and smooth, flat regions embaying topographic lows (*71*, *82*), all of which (together with chaos) comprise the mottled terrains. Some of these constructs may be small-scale examples of chaos terrains. Some, particularly the latter, may be cryovolcanic flows. Additionally, some of the features have been suggested to result from subsurface convection in the solid ice layer; this would require the ice layer thickness to exceed 10 to 30 km (depending on the ice grain size) (*82*, *83*).

Over the past 20 years, several researchers have attempted to pinpoint the nature of the lineament-forming stresses by comparing predicted stress fields with the observed orientation of the global lineaments. Hypotheses include global expansion, global contraction, orbital recession, polar wander of the ice shell, diurnal tidal stress, and nonsynchronous rotation (*4*, *84*); some of these hypotheses have been revisited with Galileo data. Of the possible mechanisms, nonsynchronous rotation (perhaps combined with diurnal tidal stress) is most relevant. The preferred scenario is that particular lineaments formed over a range of tidal bulge orientations within 60° of the present orientation relative to Europa's figure (*85*, *75*). This scenario implies a range of ages for these lineaments. None of the models provides a perfect fit, however, and uncertainties (such as how far the bulge rotates before fracture occurs) prevent definitive conclusions. Comparison of Galileo and Voyager images shows that the rotation is synchronous within measurement error (of about 1 part in 10^6); that is, if nonsynchronous, the period of Europa's rotation relative to the direction of Jupiter exceeds ~12,000 years (*86*).

Although Europa could be geologically active at present, searches indicate no obvious changes in landforms in the 17 years between Voyager and Galileo (*87*).

Surface and atmosphere. Europa's spectrum at wavelengths exceeding 1.5 μm shows strong water-ice absorption features, indicating that its surface is the most ice rich of the Galilean satellites. The spectral features are fit moderately well by the spectrum of pure water ice with a grain size of 100 μm, but important deviations from the ice spectrum indicate the presence of some nonice constituents (*13*). The spectral shape from 300 nm to 1 μm differs from that of Ganymede and Callisto and may be indicative of sulfur absorption (*59*); SO_2 is confirmed by a broad absorption near 280 nm (*88*, *89*). H_2O_2 has also been tentatively identified on Europa's surface from an absorption feature detected by NIMS near 3.5 μm and could result from energetic particle bombardment of the ice (*90*). Analyses of NIMS data indicate the presence of hydrated compounds concentrated at the lineaments and chaotic terrains; plausible candidates are hydrated frozen sulfuric acid and hydrated salts such as magnesium and sodium sulfates and sodium carbonates (*91*). NIMS spectra (1 to 5 μm) and solid state imager (SSI) spectra (400 nm to 1 μm) both indicate that this localized nonice material, which appears brown in the visible, is spectrally uniform on a regional to hemispheric scale (*91*, *92*). The uniformity suggests that the material derives from a well-mixed source region. Weak nonice absorptions at 4.05 and 4.25 μm have also been seen in NIMS spectra (*23*).

Detection of atomic oxygen airglow by HST ultraviolet (UV) spectra implies the presence of a tenuous atmosphere with a molecular oxygen column density of 10^{14} to 10^{15} cm^{-2} and scale height of a few hundred kilometers or less (*93*, *64*). An even more tenuous sodium atmosphere extending to 25 Europan radii has been detected from ground-based observations, which suggests that material is escaping from Europa's atmosphere (*94*). Radio occultations by Galileo also indicate the presence of an ionosphere with surface electron density of order 10^4 cm^{-3} (*95*).

Presence of an ocean. Many independent lines of evidence are most simply explained by, but do not require, the existence of a subsurface liquid water ocean [see the review in (*81*)]. The Galileo magnetic field data for several flybys are consistent with an induced dipole generated by a perfect conductor in Jupiter's time-variable magnetic field, although a fixed dipole also provides an adequate fit to the data (*17*). An induced dipole would most likely result from the existence of a conducting salty subsurface ocean. Conduction within or near Europa is also indicated by energetic particle measurements; an ocean is one explanation, although conduction in the ionosphere or subsurface solid material may also be sufficient (*96*). The suggestion that the brown nonice component contains hydrated sulfuric acid or salts is also most simply explained by supply from a salty source of liquid water, possibly an ocean. Galileo and Voyager images show that some large crustal blocks have moved relative to one another, implying an underlying ductile layer of either liquid water or soft ice (*97*). Proposed mechanisms for the formation of chaos, triple bands, and other features either require or are aided by the existence of an ocean (both for the nearby source of heat or liquid and the larger amplitude of tidal flexing relative to that without an ocean). Sev-

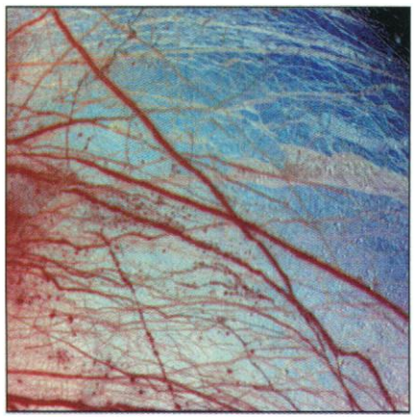

Fig. 3. False color Galileo view of icy plains and mottled terrain on Europa, assembled with images with effective wavelengths at 559, 757, and 989 nm. The plains comprise the gray and blue regions, and the mottled terrains consist of the patchy brown regions toward the left side. Also visible are numerous triple bands and other linea, which exhibit the same brown color as the mottled terrain. The brown color indicates the presence of a nonice contaminant. The image has a resolution of 1.6 to 3.3 km/pixel and spans 1260 km. The dark region in upper right corner is close to the terminator (the day-night boundary).

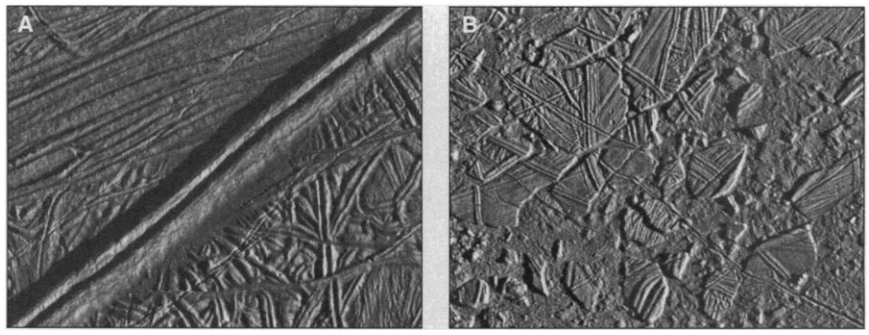

Fig. 4. High-resolution Galileo images of two of the pervasive landforms on Europa. (**A**) A region of overlapping ridges (covering a 14 km by 17 km area at 20 m/pixel). (**B**) The "chaos" terrain of disrupted crustal blocks separated by hummocky matrix (covering a region 34 km by 42 km at a resolution of 54 m/pixel). Illumination is from the right for both frames.

eral large impact features have distinct morphologies that may be indicative of impacts that penetrated through a ~6- to 15-km-thick lithosphere into a low-viscosity medium such as liquid water (*98*), although improved calculations are needed to test this hypothesis. Finally, nonsynchronous rotation, if present, probably requires decoupling of the lithosphere from the underlying silicate interior. The decoupling could occur if an ocean existed; it remains to be seen whether a ductile ice layer would also be sufficient.

Io

In 1979, Voyager observed multiple volcanic plumes on Io, and, ever since, this moon has been known to be the most endogenically active solid body in the solar system (*3*). In the intervening years, improved Earth-based observing capabilities including HST, and the Infrared Telescope Facility (IRTF) in Hawaii have been used to monitor this dynamic moon. Most recently, Galileo has added to data on Io, although the highest resolution observations with Galileo will only be completed in late 1999.

Surface composition and activity. Unlike the other Galilean satellites, Io has an extremely dry surface, because of the high rate of volcanic activity and resurfacing over much of its history, and there is no evidence for water as a substantial interior constituent either. Io's spectrum is dominated by sulfur-bearing species of which only SO_2 has been unambiguously identified (*99*). Spectral evidence for oxygen, sodium, potassium, and chlorine (*100*) in extended clouds in Io's orbital vicinity indirectly implies the presence of these elements in the surface. Diffuse red deposits associated with active volcanic sites have been interpreted as amorphous elemental sulfur (*99*, *101*); furthermore, the highest lava temperatures estimated from the Voyager data were ~650 K (*102*), consistent with sulfur-rich magma. These observations led to the idea of sulfur volcanism [but see (*103*) for an early different view]. However, ground-based observations in the late 1980s and now the data from Galileo indicate that very high temperature (>1400 K) local events, with lavas comparable to or even hotter than terrestrial basaltic eruptions, are common in the volcanically active areas (*104*). This has led to a new picture of ubiquitous silicate volcanism, plausibly including magnesium- and iron-bearing (mafic) silicates, and a surface and crust that is mostly silicate (*104*, *105*); this view contrasts with early exotic ideas of a thick surface layer of sulfur.

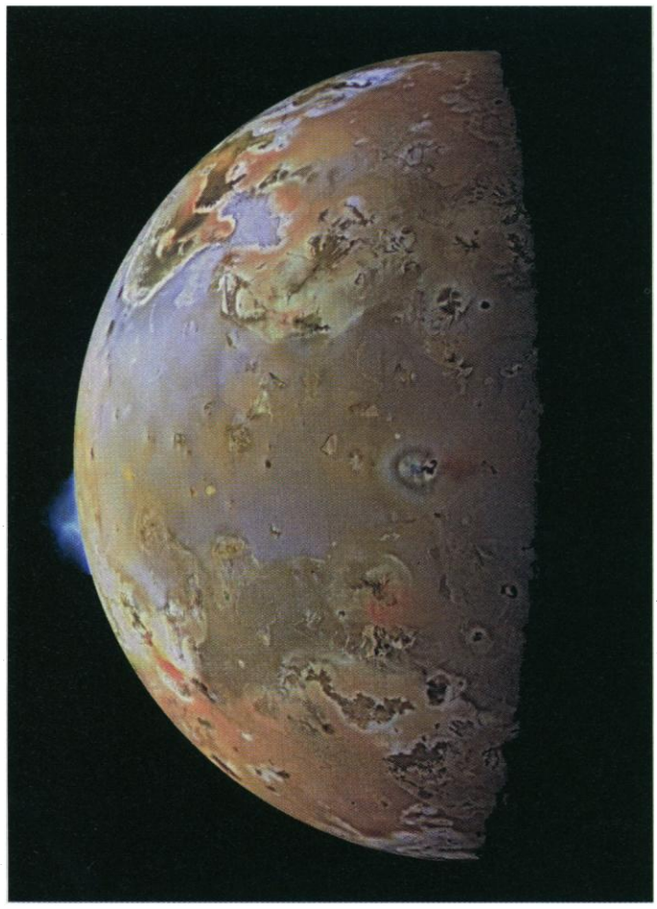

Fig. 5. A high-resolution color mosaic image of Io from Galileo data. Two volcanic plumes are visible. One on the bright limb or edge of the moon, named Pillan Patera, is 140 km high. The second plume near the terminator, the boundary between day and night, is called Prometheus; its shadow, reddish in color, can be seen extending to the right of the eruption vent (near the center of the bright and dark rings).

Io's surface is extremely varied and has unusual photometric properties, so great care is required in attributing apparent differences to time evolution rather than changes in viewing conditions. The volcanic activity on Io includes liquid lava flows, gas-rich plume eruptions, and pyroclastic eruptions (Fig. 5). The activity at local sites changes on time scales of months. New plumes appear at the rate of a few per year, and plume deposits fade away in brightness in less than twenty years. Dark areas at caldera floors seem to brighten over time in the absence of volcanism. Currently active regions appear to be concentrated at low latitudes with some evidence of excess concentration at the subjovian and antijovian locations. But the population of all volcanic centers (active or inactive) appears uniformly distributed across the surface, suggesting a globally convective asthenosphere with centers of upwelling and downwelling at spacings of several hundred kilometers (*104*, *105*).

Heat flow. The best estimate of Io's heat flow comes from ground-based IR thermal emission observations made with the IRTF from 1983 to 1993 (*106*, *107*). These data indicate that the net heat flow arises predominantly from only a few volcanic regions representing less than 10% of the surface area and indicate a heat flow of 10^{14} W averaged over 10 years. This estimate has posed a theoretical challenge, because steady-state models of tidal heating can generate at most 40% of the estimated heat flow (*7*). A popular hypothesis for reconciling the discrepancy is that Io's tidal Q and orbital eccentricity (hence tidal heating rate) vary in time because of the coupling between geophysical and orbital evolution (*108*). However, it also may be possible to resolve the discrepancy by taking account of the uncertainties in the two estimates. Veeder *et al.*'s (*106*) analysis involves modeling the size and temperature of individual emission centers. Formally, the analysis places a lower bound on Io's heat flow, but the authors do not quote an uncertainty on this lower limit. The estimated total heat flow varies less than 30% from year to year; however, the modeled heat flow from individual emission regions varies by factors of three. Moreover, the highest power is emitted at temperatures not much higher than those expected from background reradiation of absorbed sunlight, potentially increasing the uncertainties of the modeling. The theoretical maximum value is also affected by uncertainties, and it is an average over solar system history. If Jupiter's tidal Q varies in time (*109*), the present dissipation rate could be higher than the average maximum value even if Io's tidal Q is constant.

Interior structure. The moment of inertia

of Io was determined from Doppler tracking data at a close (897 km) flyby of Io during orbit insertion of Galileo (*110*), and Io's shape has been measured by analysis of the Galileo images of Io's limb (*111*). These data constrain Io's axial moment of inertia, C/MR^2, to 0.371 to 0.380, which implies a substantial degree of central condensation. Together with Io's bulk density, this value implies an interior consisting of an Fe-FeS core 35 to 60% of Io's radius in size, overlain with a silicate mantle. Details of the crustal structure of Io are inferred from the surface features. Mountains up to 16 km in height imply a silicate lithosphere with thickness exceeding ~30 km (*105*), and the characteristics of the volcanic activity may indicate a partially molten, globally convective asthenosphere underlying the lithosphere (*104*).

Magnetic field. Near Io, the jovian magnetic field strength is 1835 nT. During the Io flyby, the Galileo magnetometer measured a drop of 695 nT in the wake of Io (*112*). The data are consistent with a superposition of an Io-centered dipole on the background jovian field and antiparallel to Jupiter's dipole moment. This model Io dipole has a strength of about 1300 nT at Io's equator, making Io's magnetic moment comparable to that of the planet Mercury. A possible explanation is an intrinsic magnetic field generated by dynamo action within the molten Fe-FeS core, possibly seeded by the external jovian field (*113*). The required fluid motions may arise from instabilities induced by the tidal field of Jupiter on the spinning molten core (*114*). Alternatively, the measured field perturbation may arise from currents induced at Io by Jupiter's magnetic field (*115*).

Atmosphere and plasma torus. Io has a tenuous ~1-nanobar patchy atmosphere derived from volcanic gases, primarily SO_2 (*116*). Its spatial and temporal structure remains poorly characterized, although undoubtedly the localized volcanic sources create large horizontal pressure gradients that cause the gas to rapidly flow away from the source. Sublimation of SO_2 frost and sputtering also contribute to the generation of the atmosphere. There is spectral evidence for several neutral atomic and molecular species (O, S, Na, K, and Cl) escaping from Io and forming extended clouds along its orbit. The large escape rate (up to ~10^3 kg/s) and the large speeds (up to tens of kilometers per second) of the escaping species are probably attributable to sputtering by ions in the jovian magnetosphere (*99*). Io's atmosphere and surface contribute directly to and interact dynamically with the jovian magnetospheric plasma, which corotates with Jupiter. Atmospheric "glows" or aurorae have been observed in the UV and visible wavelengths (*117*), exemplifying some of these rich dynamical interactions. The escape and ionization of atoms from Io's atmosphere and the extended neutral clouds provide a continuous source for a plasma torus about Jupiter centered near Io's orbit (*118*).

The Galilean System

Voyager and Galileo data together with theoretical modeling indicate that tidal heating represents a powerful driver of geological activity for two, and possibly three, of the Galilean satellites. This contrasts with the situation at Earth, where the solid body tidal amplitude is <1 m and tidal dissipation is negligible relative to radiogenic heating. If Io's current heat flux represents its tidal dissipation rate, then its tidal heating exceeds the expected present-day radiogenic heat production by a factor of about 200. For Europa, the factor might be only a few (depending on uncertain parameters), whereas for the ancient resonances proposed for Ganymede the time-averaged factor is up to three (and is negligible in the current resonance). Furthermore, tidal heating can differ qualitatively from radiogenic heating because tidal heating can be spatially heterogeneous and temporally episodic. This idea has been invoked to help explain why Europa and Ganymede have such deformed surfaces despite the fact that their tidal heating rates are modest (*42*, *83*, *119*), and it may be relevant in explaining why Ganymede's geologic history diverged from Callisto's. Heterogeneous tidal heating may be able to enhance the buoyancy of convective ice diapirs, cause local thinning of the lithosphere, induce local melting, and increase local heat fluxes even when the mean flux is unremarkable; furthermore, episodic effects can lead to temporary order-of-magnitude increases in the tidal heating rate compared with the mean value. However, these ideas are speculative, and although current models are evolving rapidly, many aspects of the mechanisms involved in forming ridges and other disrupted terrains remain poorly understood. Given the possibility that both Europa and Ganymede have been affected by tidal heating, it is also not clear why the tectonic styles on Europa and Ganymede differ so drastically, particularly because evolutionary models for these satellites have similarities: Their outermost ~100 km both consist of (possibly salty) ice, they may both contain (or have contained) internal oceans below the ice, and their radiogenic heating rates are comparable.

Recent results reviewed here have highlighted the importance of micrometeoroid and energetic particle bombardment in affecting the satellite surfaces. The detection of an oxygen atmosphere and a tentative CO_2 surface feature on more than one satellite suggests that similar processes are playing a role on several of the satellites. However, differences result because the relative strength of energetic particle to micrometeoroid bombardment decreases from Io to Callisto, because Ganymede has an intrinsic magnetic field, and because the surface temperatures, composition, and endogenic resurfacing rates vary between satellites.

References and Notes

1. G. Schubert, T. Spohn, R. T. Reynolds, in *Satellites* (Univ. of Arizona Press, Tucson, AZ, 1986), pp. 224–292.
2. D. J. Stevenson, A. W. Harris, J. I. Lunine, in *Satellites* (Univ. of Arizona Press, Tucson, AZ, 1986), pp. 39–88.
3. D. B. Nash, M. H. Carr, J. Gradie, D. M. Hunten, C. F. Yoder, in *Satellites* (Univ. of Arizona Press, Tucson, AZ, 1986), pp. 629–688.
4. B. K. Lucchitta and L. A. Soderblom, in *Satellites of Jupiter* (Univ. of Arizona Press, Tucson, AZ, 1982), pp. 521–555; M. C. Malin and D. C. Pieri, in *Satellites* (Univ. of Arizona Press, Tucson, AZ, 1986), pp. 689–717.
5. W. B. McKinnon and E. M. Parmentier, in *Satellites* (Univ. of Arizona Press, Tucson, AZ, 1986), pp. 718–763.
6. B. A. Smith *et al.*, *Science* **204**, 951 (1979); B. A. Smith *et al.*, *ibid.* **206**, 927 (1979). See (*10*) for an opposing view on possible early volcanism on Callisto.
7. S. J. Peale, *Annu. Rev. Astron. Astrophys.* **37**, 37 (1999).
8. See special issue of *Space. Sci. Rev.* **60** (nos. 1 to 4) (1992) for instrument descriptions.
9. P. M. Schenk, *J. Geophys. Res.* **96**, 15,635 (1991); *ibid.* **98**, 7475 (1993).
10. ———, *ibid.* **100**, 19023 (1995).
11. W. M. Calvin and R. N. Clark, *Icarus* **104**, 69 (1993).
12. J. R. Spencer, *ibid.* **70**, 99 (1987).
13. W. M. Calvin, R. N. Clark, R. H. Brown, J. R. Spencer, *J. Geophys. Res.* **100**, 19041 (1995).
14. J. D. Anderson *et al.*, *Science* **280**, 1573 (1998).
15. Three-layer models containing an iron core cannot match the data, but a four-layer model containing an iron core, silicate mantle, mixed rock and ice mantle, and outermost ice layer has not been investigated and might fit the observations.
16. W. B. McKinnon, *Icarus* **130**, 540 (1997). However, evidence that Europa and Ganymede are nearly hydrostatic suggests caution in adopting this alternative. At the other extreme, a factor of two variation in the assumed rock/ice ratio of accreting planetesimals would allow the moment of inertia to be consistent with an undifferentiated Callisto.
17. M. G. Kivelson *et al.*, *J. Geophys. Res.* **104**, 4609 (1999); K. K. Khurana *et al. Nature* **395**, 777 (1998).
18. An ionosphere can also potentially provide conductivity, but the high electron densities required and the typically patchy nature of ionospheres suggest that this is unlikely.
19. J. S. Kargel, *Icarus* **100**, 556 (1992).
20. ———, *ibid.* **94**, 368 (1991); D. L. Hogenboom, J. S. Kargel, J. P. Ganasan, L. Lee, *ibid.* **115**, 258 (1995); D. L. Hogenboom, J. S. Kargel, P. V. Pahalawatta, *Lunar Planet. Sci. Conf.* **XXX** (1999) [CD-ROM].
21. Callisto might have accreted some ammonia hydrates, although quantification is difficult [J. I. Lunine and D. J. Stevenson, *Icarus* **52**, 14 (1982)]. A 10-km-thick ocean would have eutectic composition (hence substantial freezing point depression) if it froze from a 400-km liquid layer containing an NH_3/H_2O mole fraction of ~0.01 (~10% solar). Complete freezing of such an ocean would be prevented because convective heat loss in the overlying ice would be negligible close to the lowered freezing temperature [R. L. Kirk and D. J. Stevenson, *Icarus* **69**, 91 (1987)].
22. A. J. Friedson and D. J. Stevenson, *Icarus* **56**, 1 (1983).
23. T. B. McCord *et al.*, *J. Geophys. Res.* **103**, 8603 (1998); T. B. McCord *et al.*, *Science* **278**, 271 (1997).

24. R. Carlson *et al.*, *ibid.* **274**, 385 (1996).
25. M. L. Delitsky and A. L. Lane, *J. Geophys. Res.* **103**, 31391 (1998).
26. K. S. Noll, R. E. Johnson, M. A. McGrath, J. J. Caldwell, *Geophys. Res. Lett.* **24**, 1139 (1997); A. L. Lane, D. L. Domingue, *ibid.*, p. 1143.
27. R. W. Carlson, *Science* **283**, 820 (1999).
28. R. E. Johnson, R. M. Killen, J. H. Waite, W. S. Lewis, *Geophys. Res. Lett.* **25**, 3257 (1998).
29. J. M. Moore *et al.*, *Icarus*, in press.
30. L. M. Prockter *et al.*, *ibid.* **135**, 317 (1998).
31. A. Woronow, R. G. Strom, M. Gurnis, in *Satellites of Jupiter* (Univ. of Arizona Press, Tucson, AZ, 1982), pp. 237–276. Unpublished images from Galileo's 21st orbit hint that small craters may not be depleted in all locations.
32. J. M. Moore, M. T. Mellon, A. P. Zent, *Icarus* **122**, 63 (1996).
33. K. Zahnle, L. Dones, H. F. Levison, *ibid.* **136**, 202 (1998).
34. J. D. Anderson, E. L. Lau, W. L. Sjogren, G. Schubert, W. B. Moore, *Nature* **384**, 541 (1996).
35. M. J. S. Belton *et al.*, *Science* **274**, 377 (1996).
36. R. T. Pappalardo *et al.*, *Icarus* **135**, 276 (1998).
37. G. C. Collins, J. W. Head III, R. T. Pappalardo, *Geophys. Res. Lett.* **25**, 233 (1998).
38. R. T. Pappalardo and G. C. Collins, *Lunar Planet. Sci. Conf.* **XXX** (1999) [CD-ROM].
39. M. P. Golombek, *J. Geophys. Res.* **87** (suppl.), A77 (1982); E. M. Parmentier, S. W. Squyres, J. W. Head III, M. L. Allison, *Nature* **295**, 290 (1982).
40. J. W. Head III *et al.*, *Lunar Planet. Sci. Conf.* **XXX** (1999) [CD-ROM].
41. J. W. Head III *et al.*, *ibid.* **XXIX** (1998) [CD-ROM].
42. A. P. Showman, D. J. Stevenson, R. Malhotra, *Icarus* **129**, 367 (1997).
43. Topographic lows within grooved terrain are generally three times darker than the topographic highs (*36*). A possible cause is sloughing of a dark veneer into topographic lows during tectonism, which might expose underlying bright ice and thereby explain the brightening, although the idea remains qualitative.
44. J. Patel *et al.*, *J. Geophys. Res.*, in press.
45. A necking instability refers to runaway pinching (or "necking") of thin lithospheric regions during lithospheric extension. This mechanism was evaluated as unlikely during the Voyager era, but new rheological data for ice have prompted a reanalysis, indicating that the mechanism may indeed be feasible. See (*37*); D. L. Herrick and D. J. Stevenson, *Icarus* **85**, 191 (1990); A. J. Dombard and W. B. McKinnon, in preparation.
46. G. C. Collins, J. W. Head III, R. T. Pappalardo, *Icarus* **135**, 345 (1998). The complexity of the tectonized terrains seen by Galileo and the need to extrapolate patterns to low-resolution Voyager images argue for caution in adopting a given stratigraphy, although the coherence of the inferred stress pattern does lend the proposed stratigraphy credence.
47. A. P. Showman and R. Malhotra, *Icarus* **127**, 93 (1997); R. Malhotra, *ibid.* **94**, 399 (1991).
48. W. C. Tittemore, *Science* **250**, 263 (1990); R. Greenberg, *Icarus* **70**, 334 (1987).
49. P. Goldreich and S. Soter, *Icarus* **5**, 375 (1966).
50. M. G. Kivelson *et al.*, *J. Geophys. Res.* **103**, 19,963 (1998); M. G. Kivelson *et al.*, *Geophys. Res. Lett.* **24**, 2155 (1997); M. G. Kivelson *et al.*, *Nature* **384**, 537 (1996).
51. D. A. Gurnett, W. S. Kurth, A. Roux, S. J. Bolton, C. F. Kennel, *Nature* **384**, 535 (1996).
52. D. J. Williams, B. Mauk, R. W. McEntire, *J. Geophys. Res.* **103**, 17523 (1998); D. J. Williams *et al.*, *Geophys. Res. Lett.* **24**, 2163 (1997).
53. L. A. Frank, W. R. Paterson, K. L. Ackerson, S. J. Bolton, *Geophys. Res. Lett.* **24**, 2159 (1997).
54. W. S. Kurth, D. A. Gurnett, A. Roux, S. J. Bolton, *ibid.*, p. 2167.
55. G. Schubert, K. Zhang, M. G. Kivelson, J. D. Anderson, *Nature* **384**, 544 (1996).
56. Z. Kuang and D. J. Stevenson, *Eos* **77** (fall meet. suppl.), F437 (1996).
57. The resonance must heat the core and silicate mantle to a high enough temperature that, when the resonance ends, the cooling (which is largely controlled by the silicate mantle temperature) exceeds the required value. However, the ancient resonances that have been proposed (*47*) can generate only $\sim 10^{11}$ W of mean tidal heating within the silicate layer, ~20% of current radiogenic heat production. This value is insufficient to cause a major heating of the core. Scenarios in which the heat is deposited episodically should be considered, but it is unclear that they will get around the fact that the total resonant heat budget is modest.
58. F. J. Crary and F. Bagenal, *J. Geophys. Res.* **103**, 25757 (1998).
59. J. R. Spencer, W. M. Calvin, M. J. Person, *ibid.* **100**, 19049 (1995); W. M. Calvin and J. R. Spencer, *Icarus* **130**, 505 (1997).
60. K. S. Noll, R. E. Johnson, A. L. Lane, D. L. Domingue, H. A. Weaver, *Science* **273**, 341 (1996).
61. A. R. Hendrix, C. A. Barth, C. W. Hord, *J. Geophys. Res.* **104**, 14169 (1999).
62. W. M. Calvin, R. E. Johnson, J. R. Spencer, *Geophys. Res. Lett.* **23**, 673 (1996); R. A. Vidal, D. Bahr, R. A. Baragiola, M. Peters, *Science* **276**, 1839 (1997); M. T. Sieger, W. C. Simpson, T. M. Orlando, *Nature* **394**, 554 (1998); R. A. Baragiola and D. A. Bahr, *J. Geophys. Res.* **103**, 25865 (1998); R. E. Johnson, *ibid.* **104**, 14179 (1999); R. A. Baragiola, C. L. Atteberry, D. A. Bahr, M. Peters, *ibid.*, p. 14183.
63. R. E. Johnson and W. A. Jesser, *Astrophys. J.* **480**, L79 (1997).
64. D. T. Hall, P. D. Feldman, M. A. McGrath, D. F. Strobel, *ibid.* **499**, 475 (1998).
65. C. A. Barth *et al.*, *Geophys. Res. Lett.* **24**, 2147 (1997); L. A. Frank, W. R. Paterson, K. L. Acherson, S. J. Bolton, *ibid.*, p. 2151.
66. D. L. Domingue, A. L. Lane, R. A. Beyer, *ibid.* **25**, 3117 (1998).
67. A. L. Lane, R. M. Nelson, D. L. Matson, *Nature* **292**, 38 (1981); M. Ockert, R. Nelson, A. Lane, D. Matson, *Icarus* **70**, 499 (1987); B. Buratti and M. Golombek, *ibid.* **75**, 437 (1988).
68. R. T. Reynolds and P. M. Cassen, *Geophys. Res. Lett.* **6**, 121 (1979); P. M. Cassen, S. J. Peale, R. T. Reynolds, in *Satellites of Jupiter* (Univ. of Arizona Press, Tucson, AZ, 1982), pp. 93–128.
69. P. Cassen, R. T. Reynolds, S. J. Peale, *Geophys. Res. Lett.* **6**, 731 (1979); P. Cassen, S. J. Peale, R. T. Reynolds, *ibid* **7**, 987 (1980); S. W. Squyres, R. T. Reynolds, P. M. Cassen, S. J. Peale, *Nature* **301**, 225 (1983); G. W. Ojakangas and D. J. Stevenson, *Icarus* **81**, 220 (1989).
70. J. D. Anderson *et al.*, *Science* **281**, 2019 (1998); J. D. Anderson, E. L. Lau, W. L. Sjogren, G. Schubert, W. B. Moore, *ibid.* **276**, 1236 (1997).
71. R. Greeley *et al.*, *Icarus* **135**, 4 (1998).
72. P. E. Geissler *et al.*, *ibid.*, p. 107.
73. M. H. Carr *et al.*, *Nature* **391**, 363 (1998); N. A. Spaun, J. W. Head, G. C. Collins, L. M. Prockter, R. T. Pappalardo, *Geophys. Res. Lett.* **25**, 4277 (1998).
74. R. Greenberg *et al.*, *Icarus*, in press.
75. R. Greenberg *et al.*, *ibid.* **135**, 64 (1998).
76. R. Sullivan *et al.*, *Geol. Soc. Am. Abstr. Program* **29**, A312 (1997).
77. G. D. Crawford and D. J. Stevenson, *Icarus* **73**, 66 (1988).
78. J. W. Head *et al.*, *Lunar Planet. Sci. Conf.* **XXIX** (abstract 1414), (1998) [CD-ROM].
79. S. A. Fagents, R. Greeley, R. J. Sullivan, R. T. Pappalardo, L. M. Prockter, in preparation.
80. K. K. Williams and R. Greeley, *Geophys. Res. Lett.* **25**, 4273 (1998).
81. R. T. Pappalardo *et al.*, *J. Geophys. Res.*, in press.
82. R. T. Pappalardo *et al.*, *Nature* **391**, 365 (1998).
83. W. B. McKinnon, *Geophys. Res. Lett.* **26**, 951 (1999).
84. A. C. Leith and W. B. McKinnon, *Icarus* **120**, 387 (1996); P. Helfenstein and E. M. Parmentier, *ibid.* **61**, 175 (1985); A. S. McEwen, *Nature* **321**, 49 (1986).
85. P. E. Geissler *et al.*, *Nature* **391**, 368 (1998).
86. G. Hoppa *et al.*, *Icarus* **137**, 341 (1999).
87. C. B. Phillips *et al.*, in preparation.
88. K. S. Noll, H. A. Weaver, A. M. Gonnella, *J. Geophys. Res.* **100**, 19057 (1995).
89. D. L. Domingue and A. L. Lane, *Geophys. Res. Lett.* **25**, 4421 (1998).
90. R. W. Carlson *et al.*, *Science* **283**, 2062 (1999).
91. T. B. McCord *et al.*, *J. Geophys. Res.* **104**, 11827 (1999); T. B. McCord *et al.*, *Science* **280**, 1242 (1998); R. W. Carlson, R. E. Johnson, M. S. Anderson, *Science* **286**, 97 (1999).
92. B. E. Clark *et al.*, *Icarus* **135**, 95 (1998).
93. D. T. Hall, D. F. Strobel, P. D. Feldman, M. A. McGrath, H. A. Weaver, *Nature* **373**, 677 (1995).
94. M. E. Brown and R. E. Hill, *ibid.* **380**, 229 (1996).
95. A. J. Kliore, D. P. Hinson, F. M. Flasar, A. F. Nagy, T. E. Cravens, *Science* **277**, 355 (1997); J. Saur, D. F. Strobel, F. M. Neubauer, *J. Geophys. Res.* **103**, 19947 (1998).
96. C. Paranicas, A. F. Cheng, D. J. Williams, *J. Geophys. Res.* **103**, 15001 (1998).
97. R. Sullivan *et al.*, *Nature* **391**, 371 (1998); R. T. Pappalardo and R. J. Sullivan, *Icarus* **123**, 557 (1996); P. M. Schenk and W. B. McKinnon, *ibid.* **79**, 75 (1989).
98. J. M. Moore *et al.*, *Icarus* **135**, 127 (1998); E. P. Turtle, C. P. Phillips, A. S. McEwen, J. M. Moore, R. Greeley, *Lunar. Planet. Sci. Conf.* **XXIX** (1998) [CD-ROM]. The impact structures allegedly associated with puncture through the lithosphere are extremely flat at the scale of the whole feature, often contain several concentric ridges or troughs, and lack raised rims, central peaks, and central pits characteristic of craters formed by impact into solid ice or rock.
99. J. R. Spencer and N. M. Schneider, *Annu. Rev. Earth Planet. Sci.* **24**, 125 (1996).
100. M. Küppers and N. M. Schneider, in preparation.
101. J. R. Spencer *et al.*, *Icarus* **127**, 221 (1997); J. I. Moses and D. B. Nash, *ibid.* **89**, 277 (1991); A. S. McEwen, *ibid.* **73**, 385 (1988); R. Steudel *et al.*, *J. Geophys. Res.* **91**, 4971 (1986).
102. J. C. Pearl and W. M. Sinton, in *Satellites of Jupiter*, D. Morrison, Ed. (Univ. of Arizona Press, Tucson, AZ, 1982), pp. 724–755.
103. M. H. Carr, *J. Geophys. Res.* **91**, 3521 (1986).
104. A. S. McEwen *et al.*, *Science* **281**, 87 (1998); A. S. McEwen *et al.*, *Icarus* **135**, 181 (1998); J. R. Spencer *et al.*, *Geophys. Res. Lett.* **24**, 2451 (1997).
105. M. H. Carr *et al.*, *Icarus* **135**, 141 (1998); P. M. Schenk and M. H. Bulmer, *Science* **279**, 1514 (1998).
106. G. J. Veeder *et al.*, *J. Geophys. Res.* **99**, 17095 (1994).
107. D. L. Blaney *et al.*, *Icarus* **113**, 220 (1995); D. L. Blaney *et al.*, *Geophys. Res. Lett.* **24**, 2459 (1997).
108. R. Greenberg, in *Satellites of Jupiter*, D. Morrison, Ed. (Univ. of Arizona Press, Tucson, AZ, 1982), pp. 65–92; G. W. Ojakangas and D. J. Stevenson, *Icarus* **66**, 341 (1986).
109. P. J. Ioannou and R. S. Lindzen, *Astrophys. J.* **406**, 266 (1993).
110. J. D. Anderson, W. L. Sjogren, G. Schubert, *Science* **272**, 709 (1996).
111. P. C. Thomas *et al.*, *Icarus* **135**, 175 (1998).
112. M. G. Kivelson *et al.*, *Science* **273**, 337 (1996).
113. U. Weinbruch and T. Spohn, *Planet. Space Sci* **43**, 1045 (1995); G. R. Sarson, C. A. Jones, K. Zhang, G. Schubert, *Science* **276**, 1106 (1997); G. R. Sarson, C. A. Jones, K. Zhang, *Phys. Earth Planet. Inter.* **111**, 47 (1999).
114. R. R. Kerswell and W. V. R. Malkus, *Geophys. Res. Lett.* **25**, 603 (1998).
115. L. A. Frank *et al.*, *Science* **274**, 394 (1996); J. A. Linker, K. K. Khurana, M. G. Kivelson, R. J. Walker, *J. Geophys. Res.* **103**, 19867 (1998).
116. E. Lellouch, *Icarus* **124**, 1 (1996).
117. F. L. Roesler *et al.*, *Science* **283**, 353 (1999); P. E. Geissler *et al.*, *ibid.* **285**, 870 (1999).
118. The detailed dynamics, including transport processes and energy flow within the plasma torus, constitute a large subject beyond the scope of the present article; the reader is referred to (*99*) and F. J. Crary *et al.* [*J. Geophys. Res.* **103**, 29359 (1998)] for recent results.
119. D. J. Stevenson, in *Europa Ocean Conference* (San Juan Institute, San Juan Capistrano, CA, 1996), pp. 69–70.
120. M. E. Davies *et al.*, *Icarus* **135**, 372 (1998).
121. F. M. Neubauer, *J. Geophys. Res.* **103**, 19843 (1998).

122. We thank T. E. Dowling, W. B. McKinnon, R. T. Pappalardo, P. Schenk, N. Schneider, J. Spencer, J. Stansberry, and D. J. Stevenson for discussions. This work was supported by NASA.